Radical Cation of Naphthalene on H−ZSM-5 Zeolite and in $CFCl_3$ Matrix. A Theoretical and Experimental EPR, ENDOR, and ESEEM Study†

Roland Erickson,* Nikolas P. Benetis, Anders Lund, and Mikael Lindgren

Chemical Physics Laboratory, Department of Physics and Measurement Technology, IFM, Linköping University, S-581 83 Linköping, Sweden

Received: October 17, 1996; In Final Form: January 14, 1997⊗

The naphthalene radical cation generated from the corresponding neutral compound by UV- or X-irradiation on H−ZSM-5 zeolite and in frozen $CFCl_3$ solution has been studied by EPR, ENDOR, and ESEEM spectroscopies. The *g* and ring proton hyperfine (hf) tensors have been determined and are identical in the two media, within experimental error. The isotropic hf couplings of the two sets of four equivalent protons are $|a(1)| = 16.4$ and $|a(2)| = 4.7$ MHz (0.587 and 0.167 mT, respectively). Semiempirical calculations of isotropic and dipolar hf couplings are found to be in good agreement with experiment. The hf tensors obtained for the radical cation of naphthalene-d_8 were analogous to those of the protonated compound, scaled by the gyromagnetic ratio, γ_H/γ_D. The nuclear quadrupole interaction (nqi) tensors of the deuterium nuclei were also determined by ESEEM, being the only resolved method for the present nqi strength.

Introduction

In contrast to many other radical cations of aromatic compounds, the cations benzene$^{\bullet+}$, biphenyl$^{\bullet+}$, and naphthalene$^{\bullet+}$ are difficult to stabilize and study in solution. However, they can be prepared in rigid matrixes of certain halocarbons or on surfaces of zeolites or silica gel.[1−8] The EPR (electron paramagnetic resonance) spectra from these disordered samples suffer from limited resolution. For biphenyl$^{\bullet+}$ the higher resolution of ENDOR (electron nuclear double resonance) spectroscopy has greatly facilitated investigations of the ring proton hyperfine tensors in disordered solids.[6] In the present work on naphthalene$^{\bullet+}$ in $CFCl_3$ matrix and on H−ZSM-5 zeolite, both ENDOR and ESEEM (electron spin echo envelope modulation) spectroscopies are applied to increase the spectral resolution.

An EPR observation of surface-adsorbed naphthalene$^{\bullet+}$ on silica gel has been reported previously,[3] but no spectral interpretation was made. Hyperfine data of naphthalene$^{\bullet+}$ have been determined in two previous investigations[8,9] but with different results. An investigation in boric acid glass by Owen and Vincow[9] showed a spectrum of limited resolution. Analysis of the hyperfine (hf) tensors suggested isotropic contributions of $a(1) = -0.54$ and $a(2) = -0.162$ mT (−15.13 and −4.48 MHz) for the two groups of equivalent protons 1,4,5,8 and 2,3,6,7, respectively; see Scheme 1. The absolute values are close to those of the radical anion $|a(1)| = 0.495$ and $|a(2)| = 0.185$ mT (−13.87 and −5.19 MHz),[10] as expected from the pairing theorem.[11] A combined EPR and ENDOR study by Gerson and Qin[8] of naphthalene$^{\bullet+}$ in frozen $CFCl_3$ at 140 K reported the isotropic contributions $a(1) = -0.74$ and $a(2) = -0.187$ mT (−20.74 and −5.24 MHz, respectively). The small coupling $a(2)$ is near the value of the negative ion. But the ratio of $a^+(1)/a^-(1) = -0.74/-0.495 = 1.49$ is somewhat larger than comparable alternant hydrocarbons.[3] For biphenyl[6] the ratio a^+_{para}/a^-_{para} is 0.632/0.546 = 1.16. The observed spectra were interpreted to be due to axially symmetric hf tensors $A_\perp(1) = -0.82$, $A_\parallel(1) = -0.58$ mT and $A_\perp(2) = -0.23$, $A_\parallel(2) = -0.10$ mT, yielding the isotropic values above. The pseudoaxial symmetry of the tensors was suggested to be caused by rapid rotation of the radical around the symmetry axis, perpendicular to the molecular plane. However, a recent study[6] of the biphenyl radical cation under similar conditions showed that the tensors were completely rhombic and in good agreement with those expected for a rigid structure. The naphthalene radical cation is of interest because of its simple structure, and a correct analysis of its electronic properties is of fundamental importance. A reinvestigation by means of EPR, ENDOR, and ESEEM in rigid matrixes is therefore warranted.

SCHEME 1: Proton Position Labeling and Molecular Coordinate System in the Naphthalene Radical Cation

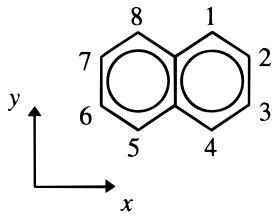

The EPR, ENDOR, and ESEEM spectra obtained in this work on naphthalene$^{\bullet+}$ are explained mainly by the significant anisotropy of the ring−proton hyperfine interactions as shown by computer simulations. Interpretation of spectra from disordered solids (termed powders in the following) is commonly hampered by broad and complex line shapes, in contrast to solution spectra. Furthermore, in ENDOR, attention must also be paid to the orientational selectivity. The ENDOR signal originates from a single position in the EPR spectrum, where the EPR resonance condition is met only for a certain range of orientations. If the powder EPR spectrum is dominated by a single anisotropic interaction, it is sometimes possible to resolve portions that correspond to a single orientation. At these positions ENDOR spectra will be single-crystal-like.[12] However, naphthalene$^{\bullet+}$ lacks a dominant anisotropic interaction, as many free radicals do, to enable observation of such single-crystal-like ENDOR spectra. Instead, ENDOR spectra are made up of a large number of superimposed orientations. Computer

† A part of this study was presented at the Royal Netherlands Academy of Sciences' Workshop on High-Frequency EPR and Electron Spin Echo Spectroscopy, Amsterdam, 1993; Abstract p 8.

⊗ Abstract published in *Advance ACS Abstracts,* March 1, 1997.

S1089-5639(96)03199-4 CCC: $14.00

simulation can take into account the orientational selectivity and predict the ENDOR spectrum at a specific position in the EPR spectrum.[13]

The two-pulse ESEEM theory involved in the simulations of the time-domain signals assumes total excitation conditions during the pulse periods of the echo experiments, which is reasonable for the hard pulses used here. On the contrary, the orientational distribution of the powder sample was treated carefully during the evolution period of the spins. Inclusion of the quadrupolar interaction of the deuterated samples was shown to be crucial for a faithful simulation of the ESEEM signals, despite being 1−2 orders of magnitude smaller compared to the hfi. Relaxation effects were disregarded in both the ENDOR and ESEEM simulations.

Experimental Section

Naphthalene-h_8 (British drug house), naphthalene-d_8 (Aldrich, >98 atom % D), and the $CFCl_3$ matrix (Aldrich) were obtained commercially and used without further purification. The H−ZSM-5 zeolite, Si/Al ratio 280, was provided by Prof. C. Rhodes, Liverpool. Samples in $CFCl_3$ were prepared using standard techniques. A small crystal of naphthalene, 0.4−0.5 mg, was placed at the bottom of a Suprasil quartz sample tube, which was then transferred to a vacuum line and pumped to 10^{-5} Torr. The tip was then immersed in liquid nitrogen, degassed $CFCl_3$ added through the vacuum line, and the tube sealed. This produced a less than 1 mol % solute mixture. Powder samples of the mixture were obtained by rapid freezing in liquid nitrogen prior to irradiation. Irradiation with X-rays was carried out at 77 K for 10 min utilizing a Philips X-ray tube (tungsten anode) operating at 70 kV and 20 mA. However, frozen samples showed evidence of being partially oriented and were thoroughly crushed in a mortar (after irradiation) under liquid nitrogen to obtain a truly polycrystalline sample. Samples on H−ZSM-5 zeolite were prepared by loading about 0.3 g of zeolite into Suprasil quartz sample tubes, o.d. 3 mm. The powder was dried in air at 160 °C for 30 min to remove most of the adsorbed water and then at 400 or 600 °C for 12−24 h. The tubes were then covered and cooled to room temperature. Immediately after cooling, a crystal of 2−3 mg of naphthalene was introduced on top of the powder, and the tube was transferred to a vacuum line, pumped to a pressure of ca. 10^{-5} Torr, and sealed. The sample was then heated in an oven at 150 °C, to let the naphthalene (mp 80 °C) diffuse into the powder. Heated samples gave negligible EPR signals before X-ray irradiation or photoirradiation. Several samples were prepared this way to ensure reproducibility of the experimental results. The possibility of dissolving naphthalene in a solvent (e.g., cyclohexane) was avoided to prevent possible solvent interactions or background signals from solvent radicals. Photoirradiation was performed at 77 K with a Bruker ER 202 UV system equipped with a 180 W mercury lamp. During photoirradiation the sample was rotated every 10 min to illuminate the sample evenly. The total irradiation time was about 30 min. X-irradiated samples were irradiated as the $CFCl_3$ samples. EPR and ENDOR measurements were performed as in ref 6. The microwave frequencies (in GHz) were as follows: in Figure 1, (a) 9.6012 and (c) 9.6033; in Figure 4, (a) 9.5774 and (c) 9.5603; in Figures 5 and 6, 9.1126. All ENDOR and ESEEM spectra were obtained at the center line of the corresponding EPR spectra. ESEEM experiments were performed on a home-built pulsed ESE spectrometer described previously.[14] A two-pulse 90°−180° sequence with 25 and 50 ns pulses was applied with a repetition time of 25 ms. Sample cooling in the ESEEM experiments was performed with an Oxford ESR-9 He-flow cryostat.

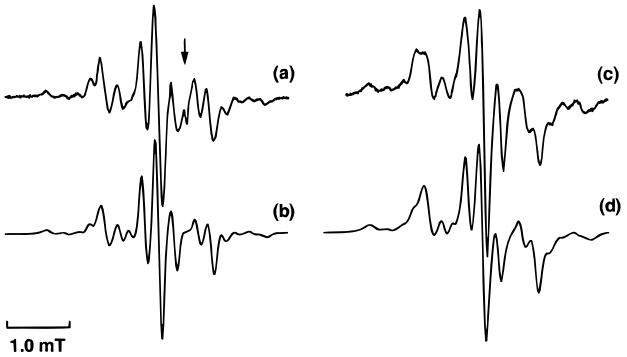

Figure 1. Comparison of experimental (a, c) and simulated (b, d) powder EPR spectra of the naphthalene-h_8 radical cation at 77 K: (a) in crushed $CFCl_3$ and (c) on H−ZSM-5 zeolite. A sharp line from irradiated quartz glass is also present in (a), indicated by the arrow. Calculated spectra employed the parameters of Table 1 and a line width of 0.09 mT (Gaussian shape in (b) and Lorentzian shape in (d)).

Theoretical Section

The EPR simulations were made with theory described previously.[15,16] The ENDOR simulation method is described in refs 6 and 13. Orientational selectivity is taken into account in the ENDOR theory. EPR transition fields and ENDOR frequencies are calculated to first order with respect to electron spin; i.e., nonsecular hyperfine terms are discarded. The Hamiltonian used in the theory is given by

$$H = \beta B\mathbf{g}S + \sum_i \{I_i\mathbf{A}_iS + I_i\mathbf{Q}_iI_i - g_i\beta_N BI_i\} \qquad (1)$$

Hyperfine, $\mathbf{A}_i$, quadrupolar, $\mathbf{Q}_i$, and nuclear Zeeman interactions, $g_i\beta_N BI_i$, of arbitrary relative magnitude and orientation can be treated. The quadrupolar tensor is not needed in the EPR and ENDOR simulations of the present system, but it is essential for ESEEM. The neglect of higher order hf terms is justified in both ENDOR and EPR since we are concerned with small hyperfine interactions (hfi) measured at high magnetic fields. The second-order correction for a single nucleus with spin $^1/_2$ is of the order of $A^2/4\nu_e$.[11] For a hyperfine coupling of 30 MHz at X-band this amounts to only 0.02 MHz . Another second-order effect occurs when there are magnetically equivalent nuclei. Cross terms may split the basic, first-order, ENDOR frequency into several transitions. In the present case the second-order splitting is too small to be resolved. The split/shift can be calculated with a formula given by Iwasaki.[17] The most drastic effect in naphthalene$^{\bullet+}$ should occur for the four equivalent protons 1,4,5,8 (see Table 1), where each first-order resonance line is shifted and split into four lines. The largest second-order splitting, which occurs for the hyperfine tensor component of −7.9 MHz, is ca. 0.023 MHz. Since the line width is 0.6 MHz, this splitting is not resolved.

The ESEEM theory developed in our laboratory is based on the density matrix formalism and is described in refs 18 and 19. The simulation program incorporates all the usual interactions in the spin Hamiltonian, inclusive nqi tensors, practically without any approximation, but it disregards the effects of the direct couplings between the nuclei. To obtain good agreement with the experimental spectra in the present case, it seemed that two particular features of the interactions were important to include into the simulation: the nonaxial symmetry of the hfi tensors and the intramolecular relative orientation of all tensors. One consequence of this is an accurate calculation of the orientation powder average. Some cases where it is important with an accurate powder averaging are discussed in ref 19 where

TABLE 1: *g* and Hyperfine Tensors Used in the EPR and ENDOR Simulations of the Radical Cation of Naphthalene-h_8 on H-ZSM-5 Zeolite and in $CFCl_3$ at 77 K

tensor	principal component	principal value[a]	direction cosines[b]		
			x	*y*	z
g	g_x	2.0028	1	0	0
	g_y	2.0024	0	1	0
	g_z	2.0025	0	0	1
A(1,4,5,8)[c]	A_x	−24.1	1	0	0
	A_y	−7.9	0	1	0
	A_z	−17.4	0	0	1
A(2,3,6,7)[c]	A_a	−7.6	±0.2970	−0.9549	0
	A_b	0.3	0.9549	±0.2970	0
	A_c	−6.7	0	0	1

[a] Hyperfine tensor values are in MHz. [b] Direction cosines are given in the molecular coordinate system defined in Scheme 1. [c] The hyperfine tensor indices correspond to the proton positions in Scheme 1.

the conditions for the validity of approximate methods, e.g., the spherical model, are given.

Results and Discussion

EPR Line Shape. The EPR spectrum of UV-irradiated naphthalene-h_8 on H−ZSM-5 zeolite at 77 K is shown in Figure 1c. This spectrum is due to naphthalene$^{\bullet+}$ and could be simulated (Figure 1d) using the parameters shown in Table 1. The molecular coordinate system and the atomic positions are shown in Scheme 1. The spectral line shape is caused mainly by the hyperfine anisotropy of the ring protons. The hf parameters were obtained from the ENDOR and ESEEM results discussed in separate sections below. The relative directions of the principal axes were taken from theoretical predictions of the tensors also discussed separately. The anisotropy in the **g** tensor used (see Table 1) is close to that calculated by Owen and Vincow[9] using the theory of Stone.[20] Inclusion of *g* anisotropy was necessary to reproduce the relative intensities of the lines. The isotropic part, $g = 2.0026 \pm 0.0003$, can be compared with the calculated value of 2.002 54.[9]

At 77 K the spectrum appears to be at the rigid limit. No line shape changes, apart from a slight line broadening, were observed when the temperature was lowered to 4 K. Above temperatures of 220 K small spectral changes were observed, perhaps caused by motion of the molecule on the surface. X-irradiated samples produced identical but stronger EPR signals (not shown) from the cation. The cation was remarkably stable on the surface and persisted up to room temperature (RT). Samples stored several days at RT still showed EPR signals from the cation of appreciable strength. A reasonable conclusion is that the diffusion of naphthalene$^{\bullet+}$ in the zeolite must be restricted, or it would be difficult to explain the high stability. We have found no spectroscopic information on whether the cation is located on the exterior surface or in the interior of the zeolite framework. However, the restricted diffusion is easier to explain whether the cation is located in the interior rather than on the exterior surface. Also, recent results obtained by X-ray diffraction on neutral naphthalene in H−ZSM-5 zeolite have given detailed information on the adsorption site.[21] In the zeolite 10-membered oxygen rings form a set of straight, parallel channels intersected by a set of zigzag channels. The naphthalene molecules were found to adsorb preferentially at the channel intersections in the interior. Possibly the radical cations are stabilized near these positions.

The EPR spectrum of X-irradiated frozen solution of naphthalene in $CFCl_3$ is presented in Figure 1a. The sample had been crushed under liquid nitrogen to obtain a proper polycrystalline matrix. Prior to crushing the samples showed orientational dependence when rotated in the spectrometer magnet, as exemplified in Figure 2. Repeated attempts to obtain polycrystalline samples without crushing failed. Most likely, the microcrystallites were too large or not entirely disordered to produce a truly polycrystalline spectrum. After crushing, the EPR spectrum was insensitive to the sample orientation. Thus, in $CFCl_3$ attention must be paid to ensure that truly disordered samples are obtained. The orientation effect in $CFCl_3$ has previously been observed for benzene$^{\bullet+}$ (X-ray-irradiated benzene/$CFCl_3$) by Iwasaki et al.[22] and for acetone$^{\bullet+}$ (γ-ray-irradiated acetone/$CFCl_3$) by Shida et al.[23] To our knowledge, the orientation effect is unique to $CFCl_3$ among the halocarbons used in EPR investigations. The amount of order/disorder seems to depend on, among other things, type of solute, solute concentration, and freezing speed. For benzene, if frozen slowly

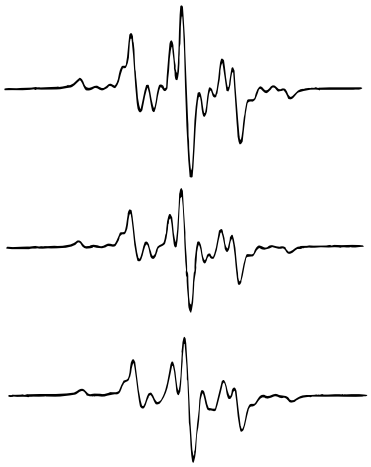

Figure 2. EPR spectra of the naphthalene radical cation in $CFCl_3$ at 77 K for three different orientations of the quartz tube in the static magnetic field. The spectra were obtained prior to crushing of the sample.

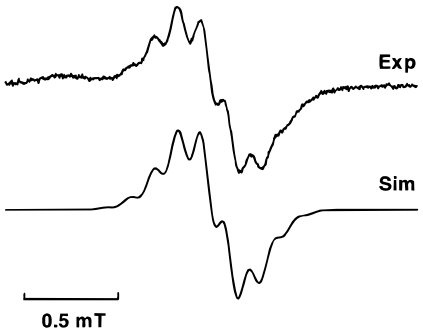

Figure 3. Comparison of experimental (upper) and simulated (lower) powder EPR spectra of the naphthalene-d_8 radical cation at 77 K in $CFCl_3$. The simulation employed the hf tensors of Table 4 and **g** tensors of Table 1 and a line width of 0.075 mT (Gaussian shape).

TABLE 2: Observed and Calculated Dipolar Hyperfine Couplings in MHz of the Naphthalene-h_8 Radical Cation

proton	principal dipolar hf coupling		
	component[a]	obsd[b] (this study)	calcd[c]
1,4,5,8	T_x	−7.66	−7.30
	T_y	8.59	9.92
	T_z	−0.94	−2.63
2,3,6,7	T_a	−2.89	−2.92
	T_b	4.97	5.28
	T_c	−2.06	−2.37

[a] Corresponding direction cosines are defined in Table 1. [b] Observed in frozen, crushed $CFCl_3$ matrix at 77 K and on H−ZSM−5 zeolite at 77 and 116 K. *c*Calculation based on McConnell's theory.32 Carbon π−spin density calculated with RHF/INDO+CI theory.

TABLE 3: Observed and Calculated Isotropic Hyperfine Couplings in MHz for the Radical Ions of Naphthalene-h_8

	radical cation						
	obsd[a] (this study)	obsd[b] (ref 8)	obsd[c] (ref 9)	calcd[d] (hfc = − 77.7ρ_π)	calcd[d] (hfc = − 72.6ρ_π)	calcd[e] (hfc = 1514ρ_σ)	radical anion obsd[f] (ref 10)
1,4,5,8	−16.44	−20.74	−15.13	−16.44	−15.36	−16.21	−13.87
2,3,6,7	−4.66	−5.24	−4.48	−4.39	−4.10	−2.87	−5.19

[a] Observed in frozen, crushed $CFCl_3$ matrix at 77 K and on H−ZSM−5 zeolite at 77 and 116 K. [b] Observed in frozen $CFCl_3$ matrix at 140 K.[8] [c] The hfc observed in frozen boric acid glass.[9] [d] Calculated with the McConnell equation. Carbon p-spin density ρ_π calculated with RHF/INDO+CI theory. [e] Proton s-spin density ρ_σ calculated with UHF/INDO theory. [f] The hfc observed when naphthalene is reduced with K in dimethoxyethane.[10]

TABLE 4: Hyperfine and Quadrupolar Tensors in MHz Used in the ESEEM Simulations for the Radical Cation of Naphthalene-d_8 in $CFCl_3$ at 28 K

					Euler angles,[a] deg		
proton	tensor	principal components			α	β	γ
1,4,5,8 (group I)	**A**	−3.70	−1.21	−2.67	0	0	0
	Q	0.025	−0.0125	−0.0125	0	0	0
2,6 (group II)	**A**	0.084	−1.17	−1.03	72.7	180	0
	Q	0.045	−0.0225	−0.0225	60	180	0
3,7 (group III)	**A**	0.084	−1.17	−1.03	107.3	180	0
	Q	0.045	−0.0225	−0.0225	120	180	0

[a] Euler angles are given with reference to the molecular coordinate system defined in Scheme 1.

at certain concentrations, it is even possible to grow transparent, single-crystal-like samples.

The spectrum obtained in crushed $CFCl_3$ is similar to that measured in the zeolite sample but is slightly better resolved. The simulation in Figure 1b was performed using the same parameters as in Figure 1d but with a Gaussian instead of Lorentzian line shape; see the figure caption. In line with the results obtained on biphenyl,[6] the naphthalene cation has similar parameters on the zeolite and in $CFCl_3$.

Analogous studies of naphthalene-$d_8^{\bullet+}$ in $CFCl_3$ and H−ZSM-5 gave additional support for the hf and **g** tensor parameters employed for the protonated compound. EPR spectra from both samples were similar but only partly resolved as shown in Figure 3 for the matrix sample. No orientational dependence of the spectrum in $CFCl_3$ could be detected, perhaps due to the limited resolution. A simulation made with the parameters from the protonated compound, but with hf tensors scaled by the gyromagnetic ratio, $\gamma_H/\gamma_D = 6.51$ (see Table 4), is also shown in Figure 3. The fit with the experimental spectrum is quite reasonable.

Powder ENDOR Simulations and Line Assignment. The ENDOR spectrum of naphthalene-$h_8^{\bullet+}$/H−ZSM-5 is presented in Figure 4a. The region of the strong matrix−proton line at 14.55 MHz has been excluded. Lines outside this zone are caused by intensity buildup corresponding to principal values of the ring proton hyperfine tensors. The ENDOR signals were acquired in the center of the EPR spectrum, a region where it is possible to observe contributions from all principal directions simultaneously. Interestingly, the line positions in the spectrum match closely those obtained for naphthalene$^{\bullet+}$/$CFCl_3$ at 140 K by Gerson and Qin,[8] although the relative intensities are different.

In agreement with the observations made on biphenyl,[6] the lines are symmetrically placed around the proton Larmor frequency, near $\nu_H \pm A_i/2$ MHz. From calculations (see below), the hf tensors of the 1,4,5,8 protons are expected to be of the α-proton type with three principal components close to 0.5*a*, *a*, and 1.5*a*, along *y*, *z*, and *x*, respectively. Here *a* is the isotropic hf coupling. Lines from all three principal directions are observable, where the lines at 26.5 and 23.2 MHz are the high-frequency lines of the A_x and A_z components of the 1,4,5,8 protons. The matching lines below ν_H are too weak to be detected, which is confirmed by the simulation in Figure 4b. The lines from A_y are located at 18.5 and 10.6 MHz and actually overlap with lines near 18 and 11 MHz from the 2,3,6,7 protons. Observation of ENDOR lines from α-protons in powders may be difficult since the signals may extend over a too large spectral region to be detectable. But, compared to a typical R−C−H_α fragment, the α-protons of the naphthalene cation radical have reduced hf couplings, due to the delocalization of the unpaired π-electron on the ring system. The smaller spread in frequencies facilitates detection of ENDOR signals.

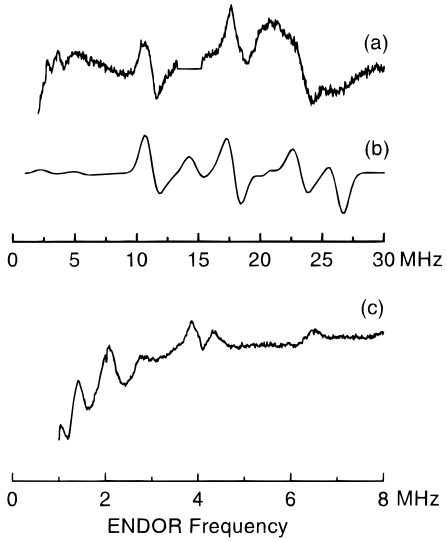

Figure 4. Experimental (a, c) and simulated (b) powder ENDOR spectra of (a) naphthalene-$h_8^{\bullet+}$ at 116 K on H−ZSM-5 zeolite and (c) naphthalene-$d_8^{\bullet+}$ at 108 K in $CFCl_3$. The region in (a) of the intense matrix line at 14.55 MHz has been excluded. ENDOR spectra were obtained at the center line of the corresponding EPR spectra in Figures 1c and 3. The simulation employed the parameters of Table 1. The EPR weight function *s* (Lorentzian shape) and the ENDOR convolution function *t* (Gaussian shape), see ref 13, had line widths of 0.07 mT and 1.0 MHz, respectively.

The hyperfine tensors of the 2,3,6,7 protons are nearly axially symmetric (see Table 1) and produce lines at 18.3, 17.9 (and 14.7 MHz which overlaps with the matrix line), with corresponding lines below ν_H. The individual lines are not resolved due to the excessive broadening. A series of simulations were performed, with hf parameters of the type predicted theoretically, to fit both the EPR and ENDOR as well as the ESEEM spectra. If the parameters were to fit the EPR spectrum, the line shape at 11 and 18 MHz in the ENDOR spectrum could only be reproduced assuming overlapping lines from several components. The simulation in Figure 4b employed the parameters in Table 1. The theory is given in ref 13. Matrix protons were excluded in the simulation. The intensity distribution is predicted fairly well in the calculated spectrum. Since relaxation and instrumental effects are neglected, a perfect fit might not be possible. Individual and anisotropic line widths may be

needed to improve the fit. For example the resonance at 26.5 MHz appears to be much broader than the other lines.

The assignment of the ENDOR lines made above also gave the best agreement with the two experimental EPR spectra (Figure 1), as well as with simple theoretical predictions of the hyperfine tensors, as discussed separately. A special detail of the EPR spectra are the five lines, including the center and the two outermost lines, which are separated by roughly 0.86 mT (24.1 MHz). The pattern could be reproduced by a hyperfine component of 0.86 mT from a principal direction common to four protons. The line at 26.5 MHz in the ENDOR spectra corresponds to the high-frequency component of this hf splitting. The splitting can be attributed to the hf component along *x* of the four protons 1,4,5,8. To fit experimental spectra the component close to *a* must be directed along *z*, as expected.

An ENDOR study of naphthalene-$d_8^{\bullet+}$/$CFCl_3$ gave additional support for the above assignment of the ENDOR signals. While the EPR spectrum in Figure 3 is only partly resolved, the ENDOR spectrum in Figure 4c shows several resolved lines. In the region near the deuterium Larmor frequency, $\nu_D = 2.23$ MHz, the lines originating from ring protons are found. The observed positions are the same as for the naphthalene-h_8 /H−ZSM-5 sample scaled with the gyromagnetic ratio, $\gamma_H/\gamma_D = 6.51$. Note also the sharp line at 4.1 MHz, confirming the presence of the corresponding but broad line at 26.5 MHz in Figure 4a. ENDOR lines below ν_D are faint or not observed because frequencies below approximately 2 MHz are difficult to detect experimentally. Investigations of naphthalene-$h_8^{\bullet+}$/$CFCl_3$ could only be performed on partly oriented samples since the crushed samples could not fit into the ENDOR quartz envelope Dewar. These spectra (not shown) gave lines at approximately the same frequencies as the polycrystalline zeolite sample.

Time-Resolved and Fourier-Transformed ESEEM Spectra. Two-pulse ESEEM measurements were performed on naphthalene-$d_8^{\bullet+}$ in $CFCl_3$ and on H−ZSM-5. Deuterated instead of protonated naphthalene was used to avoid overlap of modulations from matrix ^{19}F nuclei which lie close to the single and double proton Larmor frequencies. The pulses were chosen sufficiently long to suppress modulations from ^{19}F nuclei in the matrix. The results on the zeolite were not satisfactory due to fast relaxation of the signal. The short phase memory time allowed only a few initial modulations to be recorded.

The cation prepared in the matrix gave a much stronger signal of longer duration (Figure 5). The modulation pattern observed is due to the hf and quadrupolar couplings of the deuterium nuclei. The simulations in Figure 5a,b were performed with hf parameters from the protonated compound, scaled with the gyromagnetic ratio, $\gamma_H/\gamma_D = 6.51$. In the simulation of Figure 5a quadrupolar couplings were not included which gave an approximate fit with the experimental spectrum. Several nqi tensors, 10−100 times smaller than the hfi, were checked systematically by eye comparison of simulated and experimental time-domain signals. The initial parameters used were obtained by the above-discussed EPR line shape and the ENDOR simulations. The initial orientation of the nqi tensor was guessed by simple electrostatics appropriate to quadrupole interactions in magnetism.[24] The ESEEM modulations obtained without including the quadrupolar interaction were rather good during the first 2.5 μs of the recorded experimental time-domain signal of 5.0 μs duration. The intensity and the periodicity of the second half of the signal could not be reproduced, however, without considering the quadrupole interaction. The results of the fitting are given in Table 4. Experimental and simulated spectra including the quadrupolar parameters are given in Figure 5b. The simulation employed axially symmetric quadrupolar couplings with principal components $Q_{||} = 0.025$ and $Q_\perp = -0.0125$ MHz (deuteriums 1,4,5,8) and $Q_{||} = 0.045$ and $Q_\perp = -0.0225$ MHz (deuteriums 2,3,6,7). The individual tensors were oriented so that $Q_{||}$ was parallel to the corresponding carbon−deuterium bond. This shows that the directions of the hfi and the nqi tensors do not coincide in the *xy* plane. This geometrical factor turns out to be important for a faithful ESEEM simulation. The fit is quite reasonable and corroborates the assignment of the hf parameters in Tables 1 and 4 to naphthalene$^{\bullet+}$.

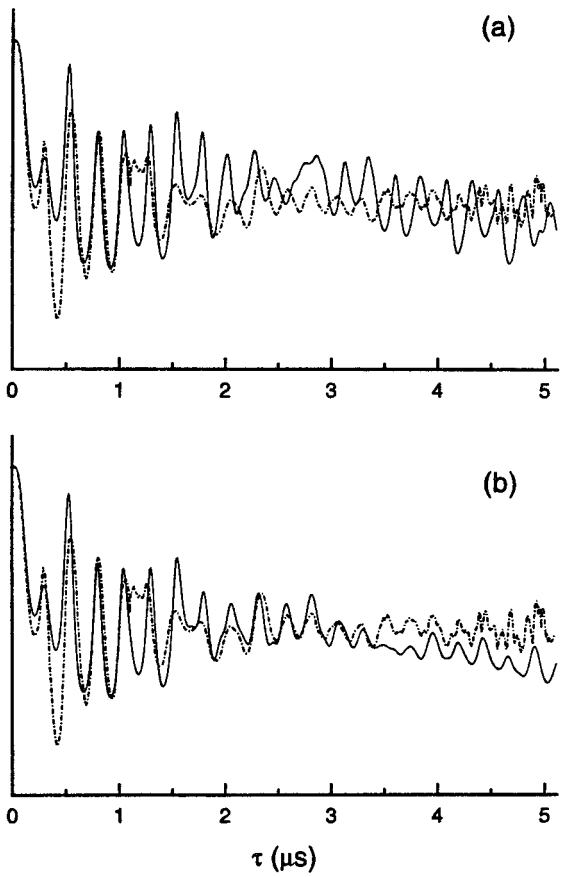

Figure 5. (a, b) Comparison of experimental (broken lines) and simulated (solid lines) time-domain powder ESEEM spectra of the naphthalene-d_8 radical cation at 28 K in $CFCl_3$. Both simulations employed the hf parameters of Table 4. In the simulation in (a) the nuclear quadrupolar couplings were zero. In the simulation in (b) the quadrupolar tensors of Table 4 were used. The individual tensors were oriented so that $Q_{||}$ was parallel to the corresponding carbon−deuterium bond. The exponential decay has been removed in both experimental curves.

Fast Fourier transformed (FFT) ESEEM spectra were partially used to check the quality of the time-domain results. The overall decay of the experimental signals was removed numerically prior to FFT treatment of the signal. A Kaiser−Bessel filter[14] was used prior to FT of the time-domain signal, as well. The poorly resolved FT spectra (cf. Figure 6), could not be used alone, however, to extract the nqi parameters.

The nqi tensors of the present system were not determined to the same degree of accuracy as the hf tensor, since the ESEEM was the only method here able to resolve the small quadrupolar interaction of the deuterons. The accuracy depends solely on the ESEEM fitting method used here, and seems to be quite good, despite that according to ref 25 1 order of magnitude of hfi could not affect the time signal significantly enough to detect any difference. The sensitivity of the time-resolved signal to the quadrupole interaction strengths was here

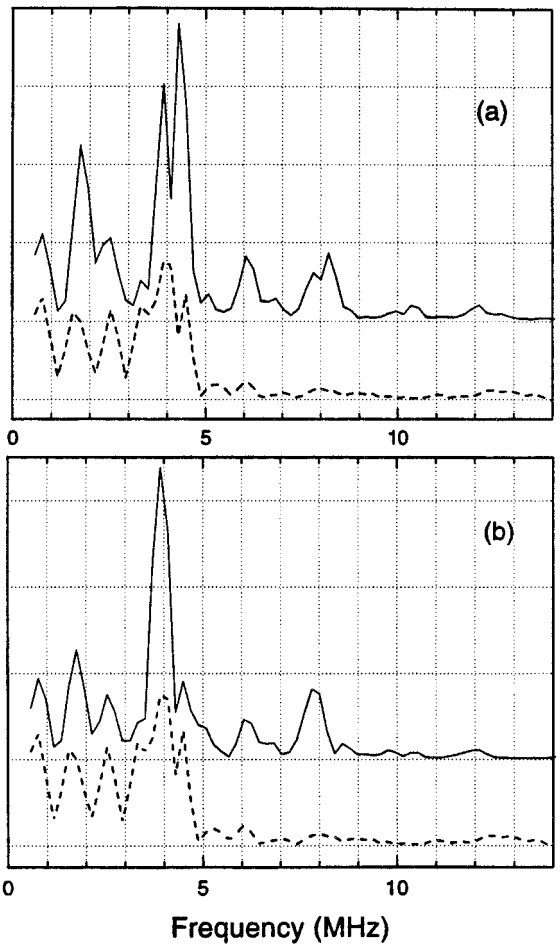

Figure 6. Fast-Fourier-transformed ESEEM spectra of the time-domain signals in Figure 5a,b. In the simulations (solid lines) the quadrupolar interaction is included only in trace b. The dashed trace corresponds to the experimental signal. A Kaiser−Bessel filter[14] was used prior to FFT of the time-domain signals. The FFT spectra were created after the determination of the parameters by using the time-domain signal.

better than 10%, meaning that observable change of the spectrum was produced for a quadrupolar magnitude change 10% at most.

The quadrupolar interactions obtained here agree reasonably well with values measured by Kurreck, Kirste, and Lubitz[26,27] on quadrupolar couplings of C−D bonds in deuterated neutral aromatic radicals dissolved in liquid crystals. The investigated species all had similar quadrupolar couplings. For 2-chlorophenalenyl-d_8 the values $Q_{zz} = 0.087 \pm 0.002$ MHz directed along the C−D bond and an asymmetry parameter $\eta = (Q_{xx} - Q_{yy})/Q_{zz} = 0.08 \pm 0.04$ (i.e., a nearly axially symmetric **Q** tensor) were reported. Here Q_{xx}, Q_{yy}, and Q_{zz} are the principal values of the quadrupole coupling tensor in eq 1. The definition of the asymmetry parameter assumes $|Q_{xx}| \leq |Q_{yy}| \leq |Q_{zz}|$.

Differences in the simulated modulations due to the **g** tensor anisotropy were visible by the present theory.[19] The **g** tensor anisotropy amounts here to 1.59 MHz, at the present field of 3250 G, which is well over the magnitude of the quadrupolar interactions. Still this magnitude is small with respect to the hfi and should not affect the nuclear modulations as directly as the hyperfine interaction. The effects of the **g** tensor anisotropy are usually disregarded in the classical ESEEM theory of Mims[28] and Dikanov.[29] Neither are explicit formulas including nonaxial hf interaction known to the authors. Anisotropy is important for π-radicals, in particular for the α-protons. The simulated time-domain signals with g anisotropy included showed enhanced homogeneous decay at the last half of the signal. Only the intensity of the beats but not their frequency was affected, however. Concluding, it should not be possible to obtain detectable experimental effects of this kind unless the magnitude of the **g** tensor anisotropy of the radical is 5-fold the one given above.

Semiempirical MO Calculations. The geometry of naphthalene$^{\bullet+}$ was optimized with the RHF/PM3 method[30] available in the MOPAC v6.00 program package. A simple single-point RHF/INDO+CI[31] calculation was performed to compute the π-electron spin density distribution in the SOMO. The calculated spin densities $\rho_{1,4,5,8} = 0.212$ and $\rho_{2,3,6,7} = 0.057$ are close to the values measured for the radical anion,[11] $\rho_{1,4,5,8} = 0.209$ and $\rho_{2,3,6,7} = 0.079$ in accordance with the pairing theorem.[11] Experimental and calculated isotropic hyperfine couplings are compared in Table 3. Our experimental values are in closer agreement with the results obtained by Owen and Vincow[9] than with those reported by Gerson and Qin.[8] Calculated values were estimated with two methods. (1) With the McConnell equation $a_i = Q\rho_i$, using the INDO calculated π-spin densities and two different values of the constant Q. The value −72.6 MHz is the value applied for benzene$^{\bullet+}$ in $CFCl_3$.[22] Apparently, this is too small for both biphenyl$^{\bullet+}$ [6] and naphthalene$^{\bullet+}$, and a value of −77.7 MHz gave better agreement with the present experimental couplings. (2) The unpaired s-electron spin densities at the protons were calculated with UHF/INDO and the hyperfine couplings estimated using a proportionality constant of 1514 MHz (54 mT).

The dipolar interaction between a ring proton and the unpaired π-electron spin density at each carbon was computed following the treatment by McConnell and Strathdee.[32] The calculated dipolar hyperfine coupling tensors of the protons, presented in Table 2, were computed using the INDO estimated spin densities. The contributions from all carbon atoms to a specific dipolar tensor were added after a transformation of the components to a common system of coordinates. The computed direction cosines are given in Table 1. The tensor for the 1,4,5,8 protons is in good agreement with experiment, resembling a typical α-proton tensor. Predicted tensors of 2,3,6,7 protons lack this α-proton character, as do the experimental tensors. The principal directions in the molecular plane are also rotated from the directions parallel and perpendicular to the C−H bond. This is expected, due to relatively larger contributions in the calculation from neighboring carbons.

Conclusions

The analysis of the powder EPR line shape of naphthalene$^{\bullet+}$ was made possible by the simultaneous use of ENDOR and ESEEM spectroscopies. Detection of powder ENDOR lines from anisotropic α-protons in naphthalene$^{\bullet+}$ was possible partly thanks to the smaller hf tensors compared to those of a typical R−C−H_α fragment. Similar observations could be expected in other organic radicals with delocalized unpaired π-electrons and anisotropic proton hf tensors. Indeed some observations are known such as in benzene$^{\bullet+}$,[7] biphenyl$^{\bullet+}$,[6] perylene$^{\bullet+}$,[33−35] the tyrosyl radical,[36,37] and *p*-benzoquinone$^{\bullet-}$.[38] The detection and analysis of the ENDOR and ESEEM powder signals were further simplified and refined by isotopic substitution of the protons by deuterons. Undesirable overlap with signals from the matrix was also avoided this way. Observed ESEEM modulations from deuterated naphthalene$^{\bullet+}$ were analyzed, and the hf and quadrupolar couplings of the ring deuteriums were obtained. This suggests that ESEEM can actually be used in investigations of free-radical structures in powders, as shown previously in a few cases.[29,37] A common application of ESEEM is otherwise to investigate intermolecular hf couplings originating from interactions with surrounding nuclei.[29]

Acknowledgment. Financial support from the Swedish Natural Science Council (NFR), the Swedish Research Council of Engineering Sciences (TFR), and the Trygger Foundation is gratefully acknowledged. We also thank U. Nordh for developing the ESEEM simulation program together with N.P.B.

References and Notes

(1) (a) Edlund, O.; Kinell, P.-O.; Lund, A.; Shimizu, A. *J. Chem. Phys.* **1967**, *46*, 3679

(2) Komatsu, T.; Lund, A. *J. Phys. Chem.* **1972**, *76*, 1727.

(3) Kinell, P.-O.; Lund, A.; Shimizu, A. *J. Phys. Chem.* **1969**, *73*, 4175.

(4) Védrine, J. C.; Auroux, A.; Bolis, V.; Dejaifve, P.; Naccache, C.; Wierzchowski, P.; Derouhane, E. G.; Nagy, J. B.; Gilson, J.-P.; van Hooff, J. H. C.; van den Berg, J. P.; Wolthuizen, J. *J. Catal.* **1979**, *59*, 248.

(5) Volodin, A. M.; Boloshov, V. A.; Konovalova, T. A. *Radicals on Surfaces*; Lund, A., Rhodes, C., Eds.; Kluwer: Dordrecht, 1995; pp 201−226.

(6) Erickson, R.; Lund, A.; Lindgren, M. *Chem. Phys.* **1995**, *193*, 89.

(7) Erickson, R.; Lindgren, M.; Lund, A.; Sjöqvist, L. *Colloids Surf., A* **1993**, *72*, 207.

(8) Gerson, F.; Qin, X.-Z. *Chem. Phys. Lett.* **1988**, *153*, 546.

(9) Owen, G. S.; Vincow, G. *J. Chem. Phys.* **1971**, *54*, 368.

(10) For a bibliography, see: *Landolt-Börnstein, Magnetic Properties of Free Radicals*; Fischer, H., Hellwege, K.-H., Eds.; Springer-Verlag: Berlin, 1980; Vol. II/9d1, pp 731−734. See for example: Gerson, F.; Müllen, K.; Wydler Ch. *Helv. Chim. Acta* **1976**, *59*, 1371.

(11) Atherton, N. M. *Principles of Electron Spin Resonance*; Ellis Horwood: Chichester, 1993; pp 98−103, 123, 193−194.

(12) Rist, G. H.; Hyde, J. S. *J. Chem. Phys.* **1970**, *52*, 4633.

(13) Erickson, R. *Chem. Phys.* **1996**, *202*, 263.

(14) Westerling, J. *ESR, ENDOR, and ESEM Studies of Free Radicals and Construction of an ESE Spectrometer*; Linköping Studies in Science and Technology, Linköping, Sweden, 1990; Dissertation No. 224.

(15) Thuomas, K.-Å.; Lund, A. *J. Magn. Reson.* **1976**, *22*, 315

(16) Lund, A.; Thuomas, K.-Å.; Maruani, J. *J. Magn. Reson.* **1978**, *30*, 505.

(17) Iwasaki, M. *J. Magn. Reson.* **1974**, *16*, 417.

(18) Benetis, N. P.; Westerling, J. *J. Magn. Reson.* **1990**, *86*, 97.

(19) Benetis, N. P.; Nordh, U. E. *Chem. Phys.* **1995**, *200*, 107.

(20) Stone, A. J. *Mol. Phys.* **1964**, *7*, 311.

(21) van Koningsveld, H.; Jansen, J. C. *Microporous Mater.* **1996**, *6*, 159.

(22) Iwasaki, M.; Toriyama, K.; Nunome, K. *J. Chem. Soc., Chem. Commun.* **1983**, 320.

(23) Ushida, K.; Shida, T. *Chem. Phys. Lett.* **1984**, *108*, 200.

(24) Slichter, C. P. *Principles of Magnetic Resonance*, 3rd ed.; Springer-Verlag: Berlin, 1990; pp 485−502.

(25) Lee, S. *J. Magn. Reson.* **1978**, *31*, 351.

(26) Kurreck, H.; Kirste, B.; Lubitz W. *Electron Nuclear Double Resonance Spectroscopy of Radicals in Solution. Application to Organic and Biological Chemistry*; VCH Publishers: Weinheim, 1988.

(27) (a) Kirste, B.; Kurreck, H.; Fey, H.-J.; Hass, Ch.; Schlömp, G. *J. Am. Chem. Soc.* **1979**, *101*, 7457. (b) Biehl, R.; Lubitz, W.; Möbius, K.; Plato, M. *J. Chem. Phys.* **1977**, *66*, 2074.

(28) Mims, W. B. *Phys. Rev. B* **1972**, *5*, 2409.

(29) Dikanov, S. A.; Tsvetkov, Y. D. *Electron Spin Echo Envelope Modulation (ESEEM) Spectroscopy*; CRC Press: Boca Raton, FL, 1992.

(30) Stewart, J. J. P. *J. Comput. Chem.* **1989**, *10*, 209.

(31) Oloff, H.; Hütterman, J. *J. Magn. Reson.* **1980**, *48*, 415.

(32) McConnell, H. M.; Strathdee, J. *Mol. Phys.* **1959**, *2*, 129.

(33) Clarkson, R. B.; Belford, R. L.; Rothenberger, K. S.; Crookham, H. C. *J. Catal.* **1987**, *106*, 500

(34) Rothenberger, K. S.; Crookham, H. C.; Belford, R. L.; Clarkson, R. B. *J. Catal.* **1989**, *115*, 430

(35) Clarkson, R. B.; Mattson, K.; Shi, W.; Wang, W.; Belford R. L. In *Radicals on Surfaces*; Lund, A., Rhodes, C., Eds.; Kluwer: Dordrecht, 1995; pp 89−117.

(36) Bender, C. J.; Sahlin, M.; Babcock, G. T.; Barry, B. A.; Chandrasekar, T. K.; Salowe, S. P.; Stubbe, J.; Lindström, B.; Pettersson, L.; Ehrenberg, A.; Sjöberg, B.-M. *J. Am. Chem. Soc.* **1989**, *111*, 8076.

(37) Warncke, K.; McCracken, J. *J. Chem. Phys.* **1994**, *101*, 1832.

(38) O'Malley, P. J.; Babcock, G. T. *J. Am. Chem. Soc.* **1986**, *108*, 3995.